ROYAL SOCIETY
OF CHEMISTRY

PAPER

Check for updates

A bimetallic nanozyme coordinated with quercetin for efficient radical scavenging and treatment of acute kidney injury†

Jiangpeng Pan,‡[a,b] Tingting Wu,‡[b] Lu Chen,‡[c] Xiaoxi Chen,[d] Chao Zhang,[b] Yanyan Wang,[a,b] Hao Li,*[d] Jiancheng Guo*[a] and Wei Jiang [ID] *[a,b,d]

Acute kidney injury (AKI), characterized by tissue inflammation and oxidative damage, is a common and potentially life-threatening complication in patients. Quercetin, a natural antioxidant, possesses diverse pharmacological properties. However, limited stability and bioavailability hinder its clinical utilization. Moreover, the application of nanotechnology in antioxidant strategies for AKI treatment faces significant knowledge gaps. These gaps stem from limited understanding of the therapeutic mechanisms and renal clearance pathways. To tackle these issues, this study aims to develop an anti-oxidation nanozyme through the coordination of quercetin (Que) with a ruthenium (Ru) doped platinum (Pt) nanozyme (RuPt nanozyme). Compared to using Que or the RuPt nanozyme alone, the combined use of Que and the nanozyme led to enhanced antioxidant activities, especially in ABTS and DPPH free radical scavenging activities. Moreover, the modified nanozyme showed remarkable efficacy in scavenging reactive oxygen species and inhibiting apoptosis in a H_2O_2-induced cellular model. Additionally, the *in vivo* study showed that the coordination-modified nanozyme effectively alleviated glycerol- and cisplatin-induced AKI by inhibiting oxidative stress. Furthermore, this nanozyme exhibited superior therapeutic efficacy when compared to free quercetin and the RuPt nanozyme. In conclusion, the findings of our study suggest that the quercetin modified RuPt nanozyme (QCN) exhibits remarkable biocompatibility and holds significant promise for the therapeutic management of AKI.

1. Introduction

Acute kidney injury (AKI) is a severe clinical syndrome that arises from multiple etiologies and is characterized by a rapid deterioration of renal function.[1–3] It is observed in roughly 10%–15% of hospitalized patients and leads to over 1.7 million fatalities each year.[1–3] The fundamental clinical diagnosis of AKI is characterized by a 50% elevation in serum creatinine (CRE) levels within a 1-week timeframe or an increase of greater than 26 µmol per L per 48 h.[4] In addition, chemotherapy drugs, such as cisplatin, and the condition known as rhabdomyolysis, are known to induce the generation of large amounts of reactive oxygen species (ROS) within renal tissues.[5,6] Subsequently, oxidative stress and inflammation resulting from the interaction between ROS and lipids, nucleic acids, and proteins lead to apoptosis and renal damage.[3,7] Thus, scavenging excess ROS within damaged renal tissue emerges as a promising strategy for addressing AKI. The utilization of natural antioxidants, including *N*-acetylcysteine and ascorbic acid, has demonstrated positive outcomes in the management of AKI.[8,9] However, the therapeutic effectiveness of the majority of drugs in addressing nephropathy is constrained by their limited efficacy resulting from a brief duration of circulation within the bloodstream and inadequate bioavailability. Hence, the development of antioxidants possessing exceptional ROS scavenging capabilities, enhanced solubility, and prolonged circulation within the body remains highly significant for the therapeutic management of AKI (Scheme 1).

Quercetin, a flavonoid that is abundantly found in various plant sources, exhibits robust antioxidant and anti-inflamma-

[a]The Research and Application Center of Precision Medicine, The Second Affiliated Hospital, Zhengzhou University, Zhengzhou, Henan, P.R. China. E-mail: weijiang@zzu.edu.cn, gjc@zzu.edu.cn

[b]Academy of Medical Sciences. Zhengzhou University, Zhengzhou, Henan, P.R. China
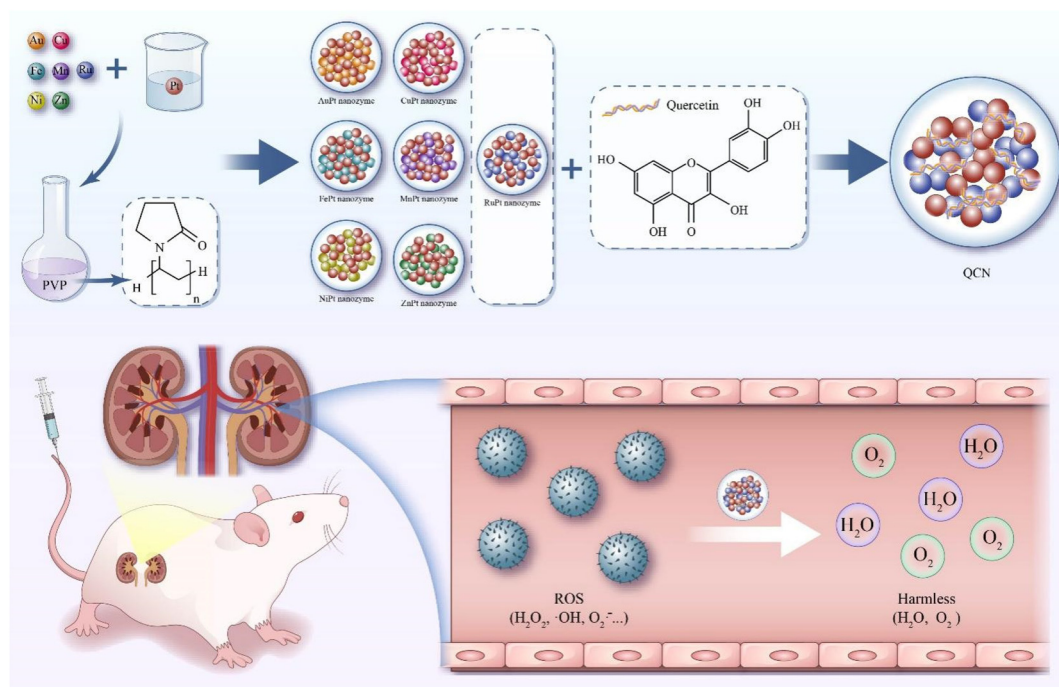
[c]Department of Cardiovascular Diseases the First Clinical Medical College. Shanxi Medical University, Taiyuan, Shanxi, P.R. China

[d]National Health Commission Key Laboratory of Cardiovascular Regenerative Medicine, Central China Fuwai Hospital of Zhengzhou University, Fuwai Central China Cardiovascular Hospital & Central China Branch of National Center for Cardiovascular Diseases, Zhengzhou, Henan, 451464, China. E-mail: leehao2004@163.com

†Electronic supplementary information (ESI) available. See DOI: https://doi.org/10.1039/d3nr05255a

‡These authors contributed equally.

Scheme 1 Schematic diagram illustrating the preparation process of QCN and QCN as antioxidants to alleviate AKI through removing excessive ROS.

tory properties.[10-15] Its therapeutic potential has been demonstrated in the management of cancer, neurological disorders, inflammatory conditions, cardiovascular ailments, and diabetes-associated diseases.[10-15] Furthermore, quercetin has the ability to exert its therapeutic impact on AKI through multiple pathways. In their study, Tan *et al.* demonstrated that quercetin exerts a protective effect against cisplatin-induced AKI by inhibiting macrophage inflammation which is sustained by Mincle/Syk/NF-κB signaling.[16] Similarly, Wang *et al.* demonstrated that quercetin effectively mitigated AKI by inhibiting ferroptosis.[17] Furthermore, it has been observed that quercetin possesses the ability to impede the development of acute kidney injury induced by the N protein of severe acute respiratory syndrome coronavirus type 2.[18] This inhibitory effect is achieved through the disruption of the Smad3-dependent G1

cell cycle arrest mechanism. However, the inadequate water solubility, permeability, and brief half-life of quercetin contribute to its rapid elimination from the bloodstream. Consequently, this leads to diminished bioavailability and restricted distribution within tissues, thereby significantly compromising the therapeutic efficacy of quercetin *in vivo.*[10,19]

Over the past few decades, there has been growing interest in nanozymes, a category of nanomaterials that exhibit enzyme-like behavior. This attention is primarily driven by their exceptional physicochemical properties. Notably, significant advancements have been made in the field of disease treatment using nanozymes, specifically in the context of AKI.[20-26] In addition, various antioxidant nanozymes have demonstrated promising effectiveness in the management of AKI. These nanozymes encompass metal complexes,[3,27-30] carbon dots,[31-33] and DNA origami.[34-37] Nanozymes offer significant advantages in enhancing bioavailability and exhibit significant potential in the therapeutic management of AKI.[38-40] The utilization of nanotechnology has facilitated the advancement of nanozymes based on quercetin, which have been designed for the treatment of various ROS-associated diseases, such as AKI.[41-43] In their study, Bao *et al.* synthesized and analyzed polyvinylpyrrolidone (PVP)-stabilized and quercetin-functionalized ultrasmall $Cu_{2-x}Se$ nanoparticles that demonstrated the ability to mitigate glycerol-induced AKI and enhance renal function by effectively scavenging ROS and upregulating the Nrf2 protein.[44] In addition, Casanova *et al.* reported the development of a micellar formulation of quercetin, which exhibited enhanced bioavailability and water solubility compared to free quercetin, and demonstrated promising

Wei Jiang is an associate professor in the Academy of Medical Science at Zhengzhou University. He obtained his Ph.D. degree at Jilin University in 2018. His research is focused on biological applications of nanozymes. He now serves as an academic editor of Exploration.

Wei Jiang

therapeutic efficacy in the treatment of cisplatin-induced AKI.[45] However, the treatment of AKI through the development of new quercetin-functionalized nanozymes that possess anti-oxidant and anti-inflammatory properties still holds promising potential.

In the present study, our primary objective was to fabricate a PVP-coated bimetallic nanozyme with a Pt catalyst, incorporating various metals such as Ru, Mn, Fe, Cu, Ni, Zn, and Au. Subsequently, the assessment of catalase-like (CAT-like), superoxide dismutase-like (SOD-like), 2,2′-azino-bis (3-ethylbenzothiazoline-6-sulfonic acid) ammonium salt (ABTS), and 1,1-diphenyl-2-picrylhydrazyl (DPPH) free radical scavenging activities facilitated the identification of a RuPt nanozyme with robust *in vitro* antioxidant capabilities. Finally, a self-assembly strategy was employed to synthesize a RuPt nanozyme that was subsequently modified with quercetin coordination (QCN). The as-obtained QCN was able to scavenge a variety of ROS

both *in vivo* and *in vitro*, thereby effectively exerting therapeutic effects on glycerol- and cisplatin-induced AKI.

2. Results and discussion

2.1 Characterization of bimetallic nanozymes and QCN

. Bimetallic nanozymes and QCN were synthesized using a facile and cost-effective approach (Fig. 1A). The obtained bimetallic nanozymes were named RuPt, MnPt, FePt, ZnPt, CuPt, NiPt, and AuPt nanozyme, respectively. The transmission electron microscopy (TEM) images showed that all six bimetallic nanozymes, with the exception of the CuPt nanozyme (~80 nm), exhibited a uniform diameter of 5–20 nm (Fig. 1B and Fig. S1†). Furthermore, the hydrodynamic dimensions of the bimetallic nanozymes, as determined by dynamic light scattering (DLS), align with the sizes observed in TEM images,
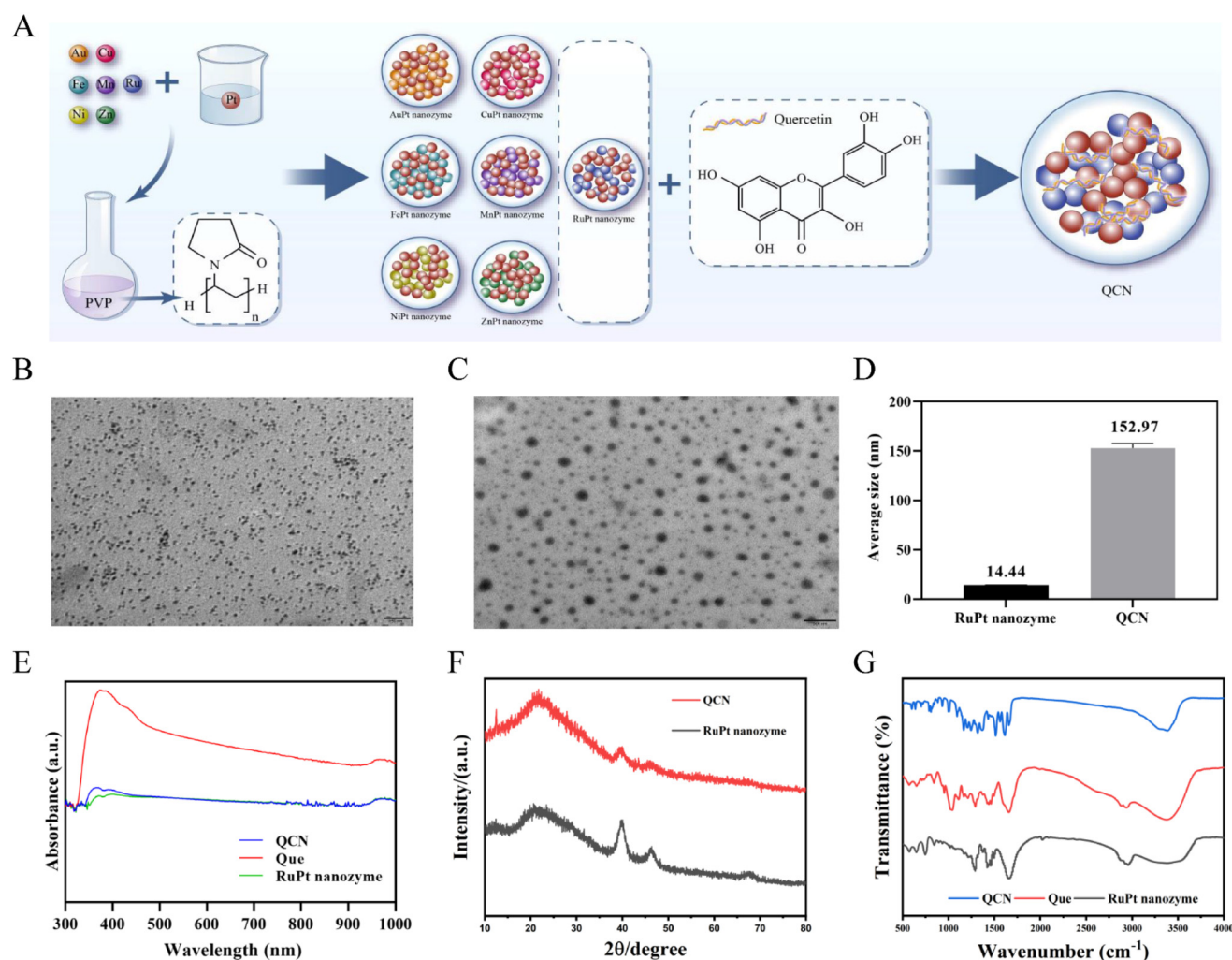

Fig. 1 Fabrication and characterization of the bimetallic nanozyme and QCN. (A) Schematic illustration of bimetallic nanozyme and QCN synthesis. (B) TEM image of theRuPt nanozyme. Scale bar: 50 nm. (C) TEM image of QCN. Scale bar: 500 nm. (D) DLS data of the RuPt nanozyme and QCN. Data represent mean ± s.d. from three independent replicates. (E) UV-vis spectra of quercetin, RuPt nanozyme and QCN. (F) XRD of the RuPt nanozyme and QCN. (G) FTIR of quercetin, RuPt nanozyme and QCN.

indicating that the bimetallic nanoparticles possess good water dispersibility (Fig. 1B and Fig. S2†). As illustrated in Fig. 1B and C, both the RuPt nanozyme and QCN exhibited a spherical shape and showed a homogeneous distribution. In addition, the findings obtained from the dynamic light scattering (DLS) analysis of the QCN indicated that the average size of the QCN particles is 152.97 nm (Fig. 1D). Additionally, as depicted in the ultraviolet-visible (UV-visible) spectrum shown in Fig. 1E, both quercetin and QCN exhibited a distinct absorption peak at approximately 380 nm, which suggests that quercetin was successfully bound to the RuPt nanozyme. Moreover, based on the X-ray diffractometry (XRD) patterns (Fig. 1F), it can be observed that the QCN exhibited peaks that were comparable to those of the RuPt nanozyme, indicating that the construction of QCN was accomplished successfully. Furthermore, the characteristic peaks observed in the Fourier transform infrared (FTIR) spectra of QCN, RuPt nanozyme, and quercetin (Fig. 1G) were highly similar in nature, which suggests that the synthesis of QCN involved the successful incorporation of both quercetin and the RuPt nanozyme. In addition, two prominent peaks in the binding energy spectrum were identified from the X-ray photoelectron spectroscopy (XPS) analysis of the obtained QCN (Fig. S3†). These were attributed to the Ru_{3d} and Pt_{4f} orbitals, respectively, indicating the oxidation states of the Ru and Pt ions present in the QCN.

2.2 Antioxidative activities of bimetallic nanozymes and QCN

The catalase-like activity exhibited by bimetallic nanozymes and QCN was assessed by measuring the alteration in O_2 content resulting from the catalysis of H_2O_2 solution. As shown in Fig. S4,† it can be observed that within a span of 10 minutes, the RuPt nanozyme exhibited the highest CAT-like activity among the seven bimetallic nanozymes. Furthermore, we conducted measurements and performed a comparative analysis of the CAT-like activity exhibited by QCN, RuPt nanozyme, and quercetin. The results depicted in Fig. 2A indicate that QCN exhibits a significant level of CAT-like activity, which further demonstrates that the modification of the RuPt nanozyme with quercetin was successfully accomplished. Thus, nanomaterials possessing catalase-like properties are likely to catalyze the decomposition of H_2O_2 into H_2O and O_2, consequently serving as a safeguard against oxidative damage to cells and tissues. In order to verify the effect of Ru on CAT-like activity, we synthesized nanozymes containing different proportions of Ru and Pt (Ru_1Pt_4 nanozyme, Ru_1Pt_2 nanozyme, Ru_1Pt_1 nanozyme, and Ru_2Pt_1 nanozyme). As shown in the Fig. S8,† the CAT-like activity of nanozymes increased with the increase of Ru content. In addition, we explored the O_2 generation of H_2O_2 solutions under different concentrations of RuPt nanozyme or H_2O_2, and the result is shown in Fig. S9.†
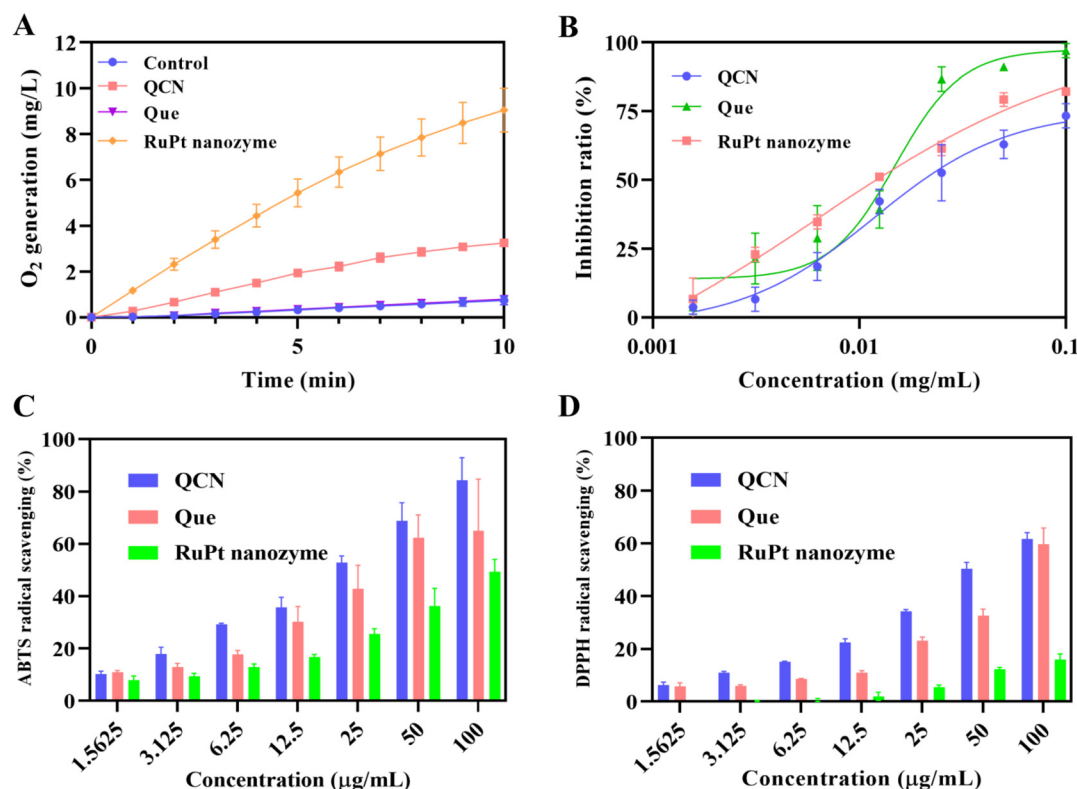

Fig. 2 ROS scavenging ability of quercetin, RuPt nanozyme and QCN. (A) CAT-like activity of quercetin, RuPt nanozyme and QCN measured by O_2 production over time. (B) SOD-like activity of quercetin, RuPt nanozyme and QCN. (C) ABTS radical scavenging ratio of quercetin, RuPt nanozyme and QCN. (D) DPPH radical scavenging ratio of quercetin, RuPt nanozyme and QCN. Data represent mean ± s.d. from three independent replicates.

In addition to the above, we examined the efficacy of bimetallic nanozymes and QCN in terms of their SOD-like activities. Superoxide anion radicals ($O_2^{\bullet-}$) were selected as the target reactive oxygen species due to their highly destructive nature. As shown in Fig. S5,† among the seven bimetallic nanozymes, the RuPt nanozyme demonstrated a superior level of SOD activity. Furthermore, it can be observed that the QCN formed by the coordination of the RuPt nanoenzyme with quercetin still retains a relatively good SOD-like activity, as depicted in Fig. 2B. One potential explanation for this outcome is that the retention of antioxidant groups in quercetin remains adequate following the modification of the RuPt nanozyme through coordination.

The ABTS radical assay was conducted to evaluate the scavenging efficacy of the seven bimetallic nanozymes towards nitrogenous radicals (Fig. S6†). The study revealed that the RuPt nanozyme demonstrated superior ABTS radical scavenging capabilities in comparison with other bimetallic nanozymes. The DPPH radical was also employed as a probe to assess the antioxidant capacity of the bimetallic nanozymes (Fig. S7†). The DPPH radical is commonly employed as a model in experiments investigating the scavenging of RNS. It exhibits a distinct absorption peak at a wavelength of 517 nm, which is observed to decrease in the presence of antioxidants. Notably, the RuPt nanozyme demonstrated the highest DPPH radical scavenging ability, when compared to the remaining six bimetallic nanozymes. Finally, the DPPH and ABTS free radical scavenging capabilities of QCN, RuPt nanozyme, and quercetin were examined. As shown in Fig. 2C and D, the ABTS and DPPH free radical scavenging ability of QCN was signifi-
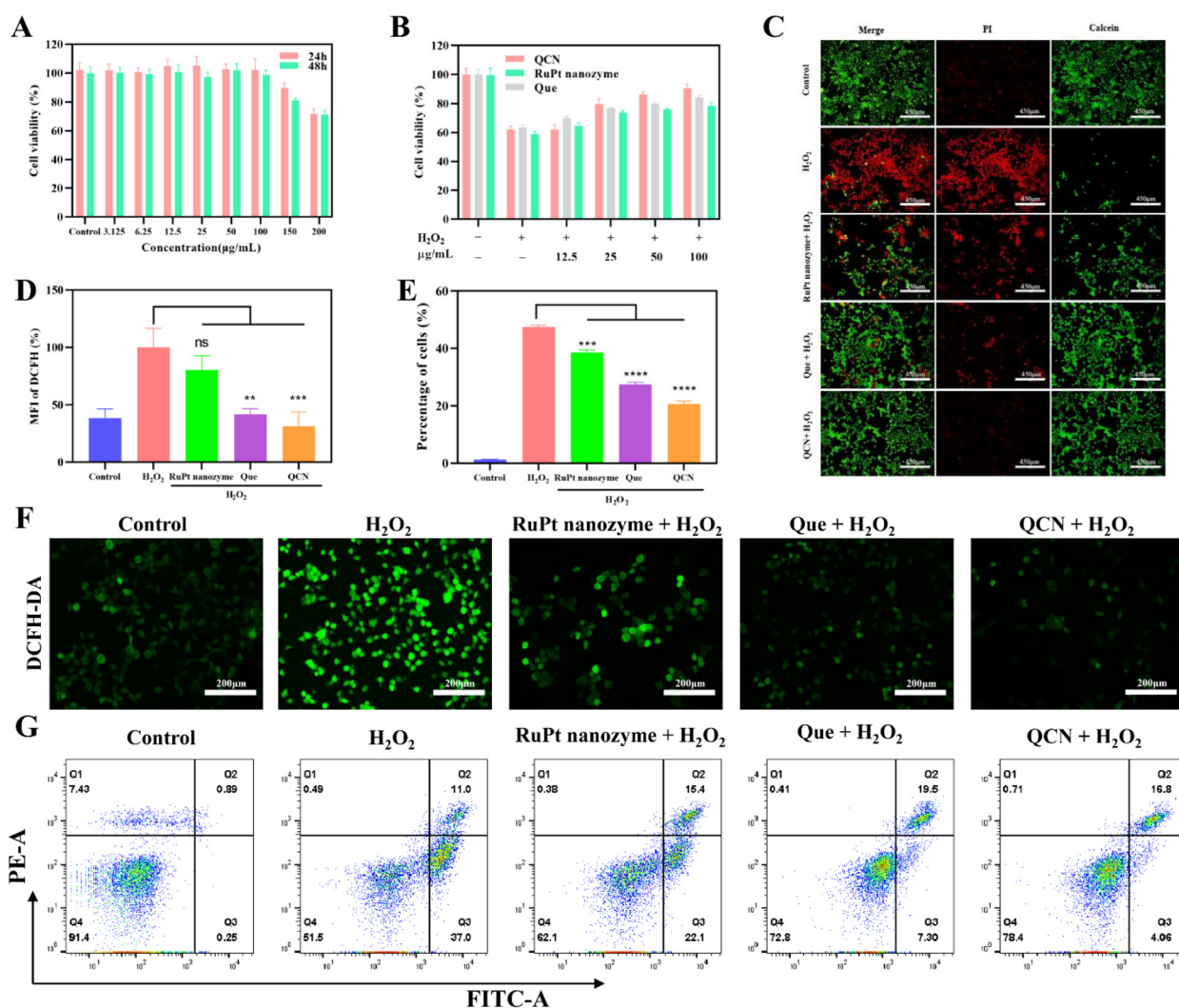

Fig. 3 QCN mediated protection of H_2O_2-stimulated cells. (A) Cell viability of HEK293 cells treated with various concentrations of QCN for 24 and 48 h as determined by CCK8 assay ($n = 5$). (B) Cell viability of HEK293 cells under H_2O_2 with/without various concentrations of quercetin, RuPt nanozyme and QCN ($n = 3$). (C) Fluorescence images of calcein AM- and PI-stained HEK293 cells. Scale bar: 450 μm. (D) Flow cytometry quantification of DFCH-DA stained HEK293 cells after different treatments. (E) Statistical analysis of apoptotic cell ratios in HEK293 cells under different treatment conditions. (F) Confocal fluorescence images of DFCH-DA stained HEK293 cells after different treatments. (G) FACS results of apoptotic cells in HEK293 cells under different treatment conditions (ns: non-significant, *$P < 0.05$, **$P < 0.01$, ***$P < 0.001$, ****$P < 0.0001$).

cantly better than that of free quercetin and the RuPt nanozyme, which suggests that QCN possesses remarkable potential for the treatment of AKI by virtue of its antioxidant capabilities.

2.3 QCN mediated protection of H_2O_2-stimulated cells

QCN exhibited robust antioxidant activity *in vitro* and demonstrated significant efficacy in safeguarding cells from H_2O_2-induced oxidative damage. Human embryonic kidney 293 (HEK293) cells were used as a model for conducting the *in vitro* studies. We verified the damage of HEK293 cells using different concentrations of H_2O_2 and finally selected a concentration of 500 μM H_2O_2 as the cell model of oxidative damage (Fig. S10†). By comparing the cytotoxicity of the four nanozymes (Ru_1Pt_4 nanozyme, Ru_1Pt_2 nanozyme, Ru_1Pt_1 nanozyme, and Ru_2Pt_1 nanozyme) and their protective effects on HEK293 cells induced by H_2O_2, the Ru_1Pt_1 nanozyme was selected as the main study object (Fig. S11, and S12†). Accordingly, we used 2-(2-methoxy-4-nitrophenyl)-3-(4-nitrophenyl)-5-(2,4-ben-

zenedisulfonic acid)-2*H*-tetrazole monosodium salt (CCK8) to evaluate the cytotoxicity of QCN. The results obtained from the CCK-8 assay indicated that the cytotoxicity of QCN towards HEK293 cells was insignificant at both 24 h and 48 h timepoints when the concentration of QCN was lower than 100 μg mL^{-1} (Fig. 3A). In addition, the results of the hemolysis experiments indicated that the hemolysis rate remained below 7% when the concentration of QCN was below 100 μg mL^{-1}, suggesting that QCN has good biocompatibility (Fig. S13†). The findings obtained from the hemolysis experiment align with prior research, indicating that QCN typically exhibits low toxicity at comparatively low concentrations (<100 μg mL^{-1}).

Cell death can be induced by excessive oxidative stress, such as prolonged exposure to H_2O_2. In order to assess the impact of QCN on cell viability induced by H_2O_2, a series of treatments were administered to the cells. These treatments included quercetin, RuPt nanozyme, and QCN. Following the administration of these treatments, the cells were exposed to H_2O_2 (500 μM), and the viability of the cells was assessed
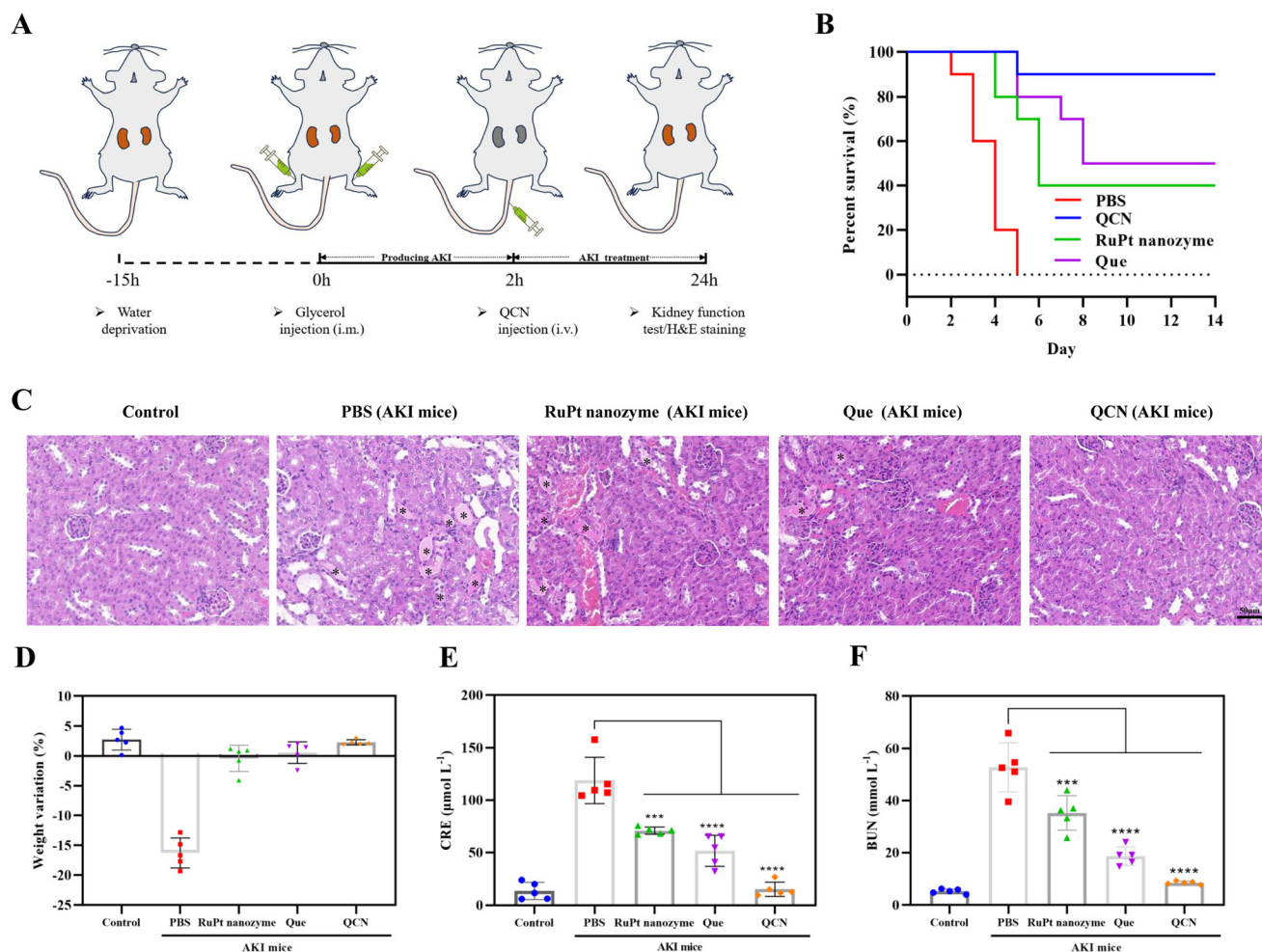

Fig. 4 Blood serum measurements and H&E staining of renal tissue after treatment with the nanozyme. (A) Preparation and treatment schedule of AKI mice. (B) Survival curves of AKI mice with different treatments. (C) H&E staining of kidney tissues from each group. (D) Weight variation of AKI mice at 24 h after treatment. (E and F) Serum levels of CRE and BUN in AKI mice at 24 h after different treatments. Data represent mean ± s.d. from five independent replicates (ns: non-significant, *P < 0.05, **P < 0.01, ***P < 0.001, ****P < 0.0001).

using the CCK-8 assay. As shown in Fig. 3B and C, the QCN treated group showed the best cell viability. Furthermore, the evaluation of cell death in HEK293 cells with QCN and/or H_2O_2 (500 μM) was conducted using the annexin V/PI apoptosis assay (Fig. 3E and G). The average percentage of apoptotic cells was 1.33% in the control group, while that in the group treated with H_2O_2 alone was 47.54%. In the quercetin treatment group, the proportion of apoptotic cells was 27.63%, while in the RuPt nanozyme treatment group it was 38.57%. Lastly, in the QCN and H_2O_2 co-treatment group, the proportion of apoptotic cells was 20.95%. All three compounds demonstrated the ability to inhibit H_2O_2-induced apoptosis, with QCN exhibiting a more pronounced inhibitory effect.

Subsequently, the 2′,7′-dichlorofluorescein diacetate (DCF) fluorescent dye was employed for the purpose of quantifying the levels of ROS within the HEK293 cells. As shown in Fig. 3F, cells preincubated with quercetin, RuPt nanozyme, and QCN exhibited lower levels of ROS than cells treated with H_2O_2 alone. The obtained quantitative results revealed that the DCF intensity of the three treatment groups with the addition of H_2O_2 was comparatively lower than that of the treatment group with H_2O_2 alone (Fig. 3D and Fig. S14†). Furthermore, it was observed through both confocal imaging and flow cytometric analysis that QCN exhibited a more pronounced impact on the reduction of intracellular ROS compared to quercetin and the RuPt nanozyme.

2.4 *In vivo* therapeutic efficacy of QCN on AKI mice

We also conducted a study to investigate the *in vivo* therapeutic effect of QCN on AKI, taking into account its impressive ability to scavenge ROS and its favorable biosafety profile. The experimental procedure involved the induction of rhabdomyolysis-induced AKI in normal mice through intramuscular injection of a 50% glycerol solution (Fig. 4A). The survival curve of mice with AKI was observed following a two-week treatment period (Fig. 4B). It was observed that the AKI model mice experienced mortality within five days. However, AKI mice treated with QCN exhibited a higher survival rate than other experimental groups. As shown in Fig. 4D, AKI mice that received QCN treatment exhibited weight gain comparable to healthy mice. Conversely, AKI mice experienced notable weight loss within a 24 h period, while AKI mice treated with quercetin and the RuPt nanozyme demonstrated a slight decrease in weight. The primary clinical characteristics of AKI are elevated levels of blood urea nitrogen (BUN) and creatinine (CRE), which serve as indicators for assessing renal excretory function. The blood biochemical analysis revealed that QCN-treated AKI mice exhibited significantly reduced levels of CRE and BUN com-
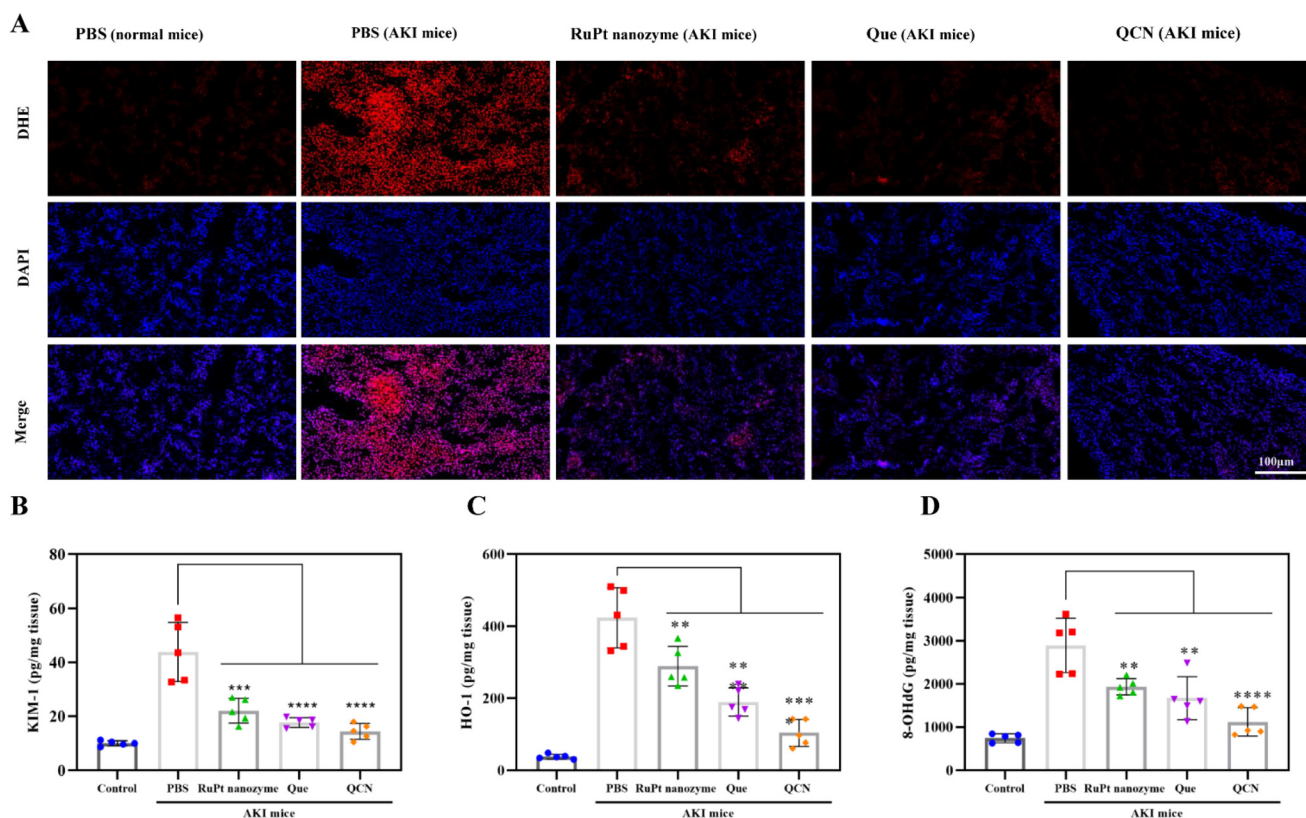

Fig. 5 Analysis of renal tissue after treatment with the nanozyme. (A) Dihydroethidium (DHE) and DAPI staining of kidney tissues from each group. Scale bar: 100 μm. KIM-1 (B) and HO-1 (C) measured in renal tissue homogenates from each group. (D) Measurement of DNA damage (8-OHdG) in renal tissue homogenates from each group. In (B–D), data represent mean $\pm$ s.d. from five independent replicates (ns: non-significant, *$P < 0.05$, **$P < 0.01$, ***$P < 0.001$, ****$P < 0.0001$).

pared to AKI mice treated with PBS, quercetin, and RuPt nanozyme (Fig. 4E and F). This suggests that QCN demonstrates remarkable effectiveness in treating glycerol-induced AKI.

Subsequently, hematoxylin and eosin (H&E) staining was conducted on kidney tissues in order to furnish conclusive evidence pertaining to the treatment of AKI. Cast refers to a material that is formed within the tubules of the kidneys as a result of the denaturation of proteins. It is commonly employed as a diagnostic marker for the presence of kidney disease. Fig. 4C shows the presence of casts (indicated by asterisks) in the kidney sections of AKI mice. Notably, AKI mice treated with QCN exhibited a reduced number of impaired structures compared to AKI mice treated with quercetin and the RuPt nanozyme. This finding provides additional evidence supporting the significant role of QCN in the prevention of AKI.

In order to conduct a more comprehensive investigation into the role of QCN *in vivo*, kidney tissues were subjected to dihydroethidium (DHE) staining. As shown in Fig. 5A, the administration of QCN to AKI mice exhibited the most effective suppression of renal ROS generation in comparison with that in the other experimental groups. Furthermore, the measurement of SOD levels, a crucial protease responsible for eliminating ROS within renal cells *in vivo*, was conducted on kidney tissue (Fig. S15†). The SOD levels in AKI mice treated with QCN were comparable to those of normal mice. Conversely, a notable reduction in SOD levels was observed in AKI mice treated with PBS. These findings suggest that QCN functions as a reducing agent, effectively scavenging ROS,

restoring SOD levels, and providing additional protection to AKI mice.

Furthermore, the levels of kidney injury molecule-1 (KIM-1) and heme oxygenase-1 (HO-1), which are recognized as significant biomarkers for kidney injury, were evaluated in the kidney tissue. In the AKI mouse model, administration of QCN resulted in kidney tissue levels of KIM-1 and HO-1 that were comparable to those observed in healthy mice (Fig. 5B and C). However, treatment of AKI mice with quercetin and the RuPt nanozyme led to a partial reduction in KIM-1 and HO-1 levels. Furthermore, an investigation was conducted to examine the potential inhibitory effects of QCN on DNA damage. In contrast to the AKI mice treated with PBS, the mice treated with QCN exhibited a significant reduction in 8-hydroxy-2′-deoxyguanosine (8-OHdG) levels in the kidneys (Fig. 5D). This reduction in 8-OHdG serves as an indicator of oxidative stress and a quantitative measure of DNA damage. The obtained results elucidate the favorable therapeutic efficacy of QCN in the context of AKI.

Based on the aforementioned encouraging outcomes, our subsequent investigation focused on assessing the effectiveness of QCN *in vivo*, in the context of the cisplatin-induced acute kidney injury (cis-AKI) model. Cisplatin is a chemotherapy drug that is commonly employed in clinical settings. It has the ability to accumulate in renal tissue and initiate apoptosis pathways, resulting in cellular damage due to oxidative stress and inflammation. Consequently, this process can lead to the development of AKI.[46] The findings of
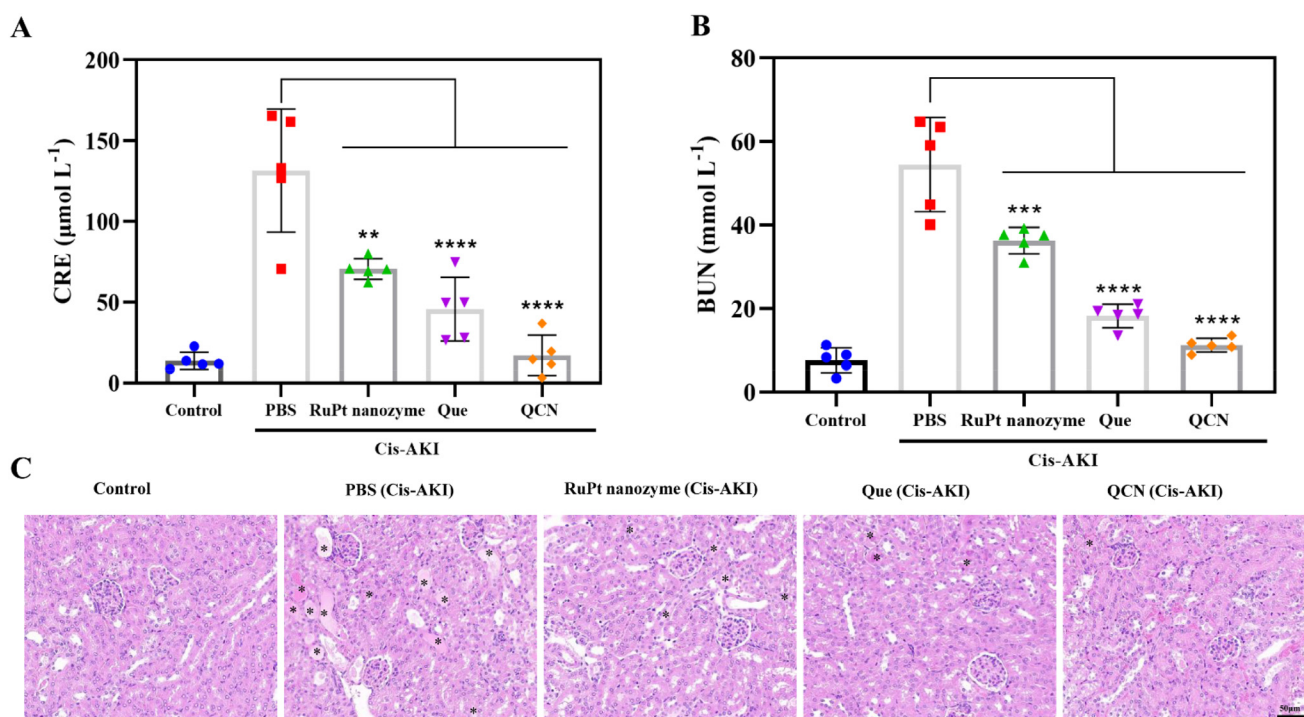

Fig. 6 *In vivo* treatment with the nanozyme for cis-AKI. (A) CRE and (B) BUN levels in the blood serum from each group. (C) H&E staining of kidney tissues from each group. In (A) and (B), data represent mean ± s.d. from five independent replicates (ns: non-significant, *$P < 0.05$, **$P < 0.01$, ***$P < 0.001$, ****$P < 0.0001$).
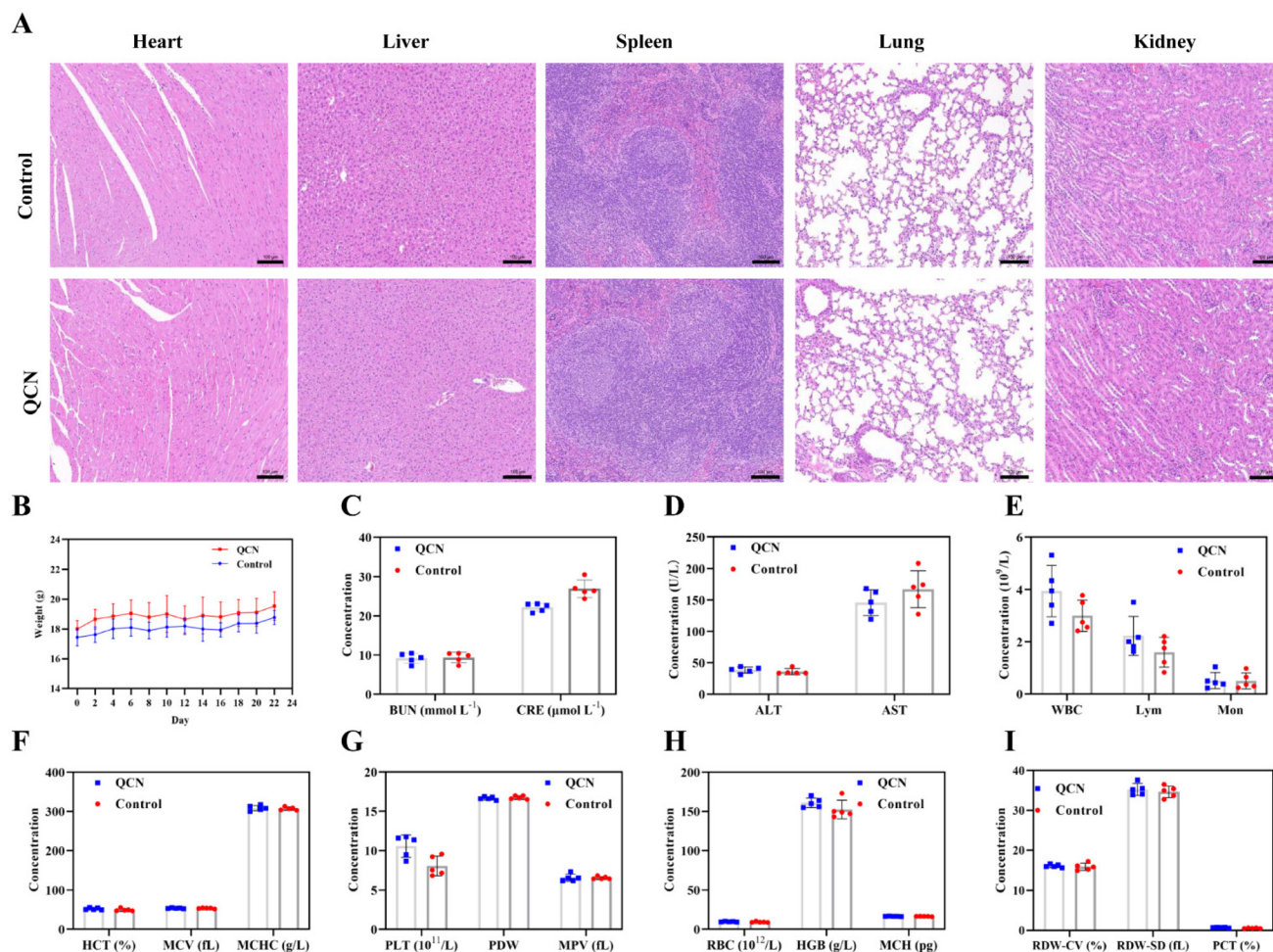
Fig. 7 *In vivo* toxicity assessment of QCN. (A) Evaluation of *in vivo* toxicity of QCN to major organs (heart, liver, spleen, lungs and kidneys) at 21 days after intravenous administration. Scale bar: 100 μm. (B) Body weight changes after intravenous injection of QCN or PBS. (C) Kidney function indicators CRE and BUN in normal mice and mice injected with QCN. (D) Liver function indicators alanine aminotransferase (ALT) and aspartate aminotransferase (AST) in normal mice and mice injected with QCN. (E−I) Serum biochemistry assay and blood panel data of normal mice and mice post QCN injection. In (B−I), data represent mean ± s.d. from five independent replicates.

our study demonstrate that QCN exhibits notable therapeutic efficacy in mice with cis-AKI. As shown in Fig. 6, the evaluation of kidney function and histological examination using H&E staining demonstrated a notable reduction in kidney damage in cis-AKI mice treated with QCN compared to those treated with PBS and other control drugs. These results provide confirmation of the therapeutic efficacy of QCN in the context of cis-AKI.

2.5 *In vivo* toxicity assessment

Subsequently, the *in vivo* toxicity of QCN was assessed following the administration of QCN *via* intravenous injection at a dosage of 20 mg kg^{-1}. The alterations in weight were consistently monitored. Twenty-one days post-injection, samples of major organs and blood were obtained. No statistically significant difference in body weight was observed between the control group and the group of mice treated with QCN (Fig. 7B). Furthermore, histological examination of major

organs using H&E staining revealed no observable adverse effects following treatment with QCN (Fig. 7A). Simultaneously, the examination of blood biochemical markers, including BUN, CRE, alanine aminotransferase (ALT), and aspartate aminotransferase (AST), indicated that the liver and kidneys exhibited normal functioning (Fig. 7C and D). The findings from all experiments consistently indicate that QCN exhibits minimal toxicity in living organisms, demonstrates favorable biocompatibility, and offers therapeutic advantages in the management of AKI.

3. Conclusions

A novel anti-oxidation nanozyme has been effectively synthesized through the coordination of quercetin with a ruthenium (Ru) doped platinum (Pt) nanozyme (referred to as RuPt nanozyme). This nanozyme holds potential for the treatment

of rhabdomyolysis- and cisplatin-induced AKI. QCN exhibiting a uniform size distribution and excellent dispersion was synthesized using a straightforward solution preparation method. The QCN enzyme exhibits multiple enzymatic activities, including CAT-like and SOD-like activities. These activities are anticipated to efficiently eliminate various ROS, such as H_2O_2, $O_2^{\cdot-}$. The protective effect of QCN on H_2O_2-induced HEK293 cells is attributed to its favorable biocompatibility and exceptional antioxidant properties. Furthermore, following the introduction of QCN into the system, the body facilitates the release of quercetin and the RuPt nanozyme from the nanoparticles into the bloodstream *via* the process of blood circulation. Quercetin functions as a naturally occurring bioactive antioxidant within the renal system, while the nanozyme composed of small-sized RuPt particles exhibits a protective effect in cases of AKI. In summary, QCN exhibits great potential as a nano-antioxidant for mitigating the effects of rhabdomyolysis- and cisplatin-induced AKI.

Ethical statement

All animal studies were conducted in accordance with the protocol approved by the Animal Ethics Committee of the Experimental Animal Center of Zhengzhou University (license No. ZZU-LAC20230526[20]).

Conflicts of interest

There are no conflicts to declare.

References

1 C. Ronco, R. Bellomo and J. A. Kellum, *Lancet*, 2019, **394**, 1949–1964.
2 J. A. Kellum, P. Romagnani, G. Ashuntantang, C. Ronco, A. Zarbock and H. J. Anders, *Nat. Rev. Dis. Primers*, 2021, **7**, 52.
3 D. Ni, D. Jiang, C. J. Kutyreff, J. Lai, Y. Yan, T. E. Barnhart, B. Yu, H.-J. Im, L. Kang, S. Y. Cho, Z. Liu, P. Huang, J. W. Engle and W. Cai, *Nat. Commun.*, 2018, **9**, 5421.
4 J. A. Kellum, C. Ronco and R. Bellomo, *Nat. Rev. Nephrol.*, 2021, **17**, 493–502.
5 K. Hosohata, *Int. J. Mol. Sci.*, 2016, **17**, 1826.
6 S. A. Lee, M. Cozzi, E. L. Bush and H. Rabb, *Am. J. Kidney Dis.*, 2018, **72**, 846–856.
7 P. Pickkers, M. Darmon, E. Hoste, M. Joannidis, M. Legrand, M. Ostermann, J. R. Prowle, A. Schneider and M. Schetz, *Intensive Care Med.*, 2021, **47**, 835–850.
8 J. Luo, T. Tsuji, H. Yasuda, Y. Sun, Y. Fujigaki and A. Hishida, *Nephrol., Dial., Transplant.*, 2008, **23**, 2198–2205.
9 U. Sadat, A. Usman, J. H. Gillard and J. R. Boyle, *J. Am. Coll. Cardiol.*, 2013, **62**, 2167–2175.
10 G. E. Batiha, A. M. Beshbishy, M. Ikram, Z. S. Mulla, M. E. Abd El-Hack, A. E. Taha, A. M. Algammal and Y. H. A. Elewa, *Foods*, 2020, **9**, 374.
11 B. Salehi, L. Machin, L. Monzote, J. Sharifi-Rad, S. M. Ezzat, M. A. Salem, R. M. Merghany, N. M. El Mahdy, C. S. Kilic, O. Sytar, M. Sharifi-Rad, F. Sharopov, N. Martins, M. Martorell and W. C. Cho, *ACS Omega*, 2020, **5**, 11849–11872.
12 H. Khan, H. Ullah, M. Aschner, W. S. Cheang and E. K. Akkol, *Biomolecules*, 2020, **10**, 59.
13 A. Rauf, M. Imran, I. A. Khan, M. Ur-Rehman, S. A. Gilani, Z. Mehmood and M. S. Mubarak, *Phytother. Res.*, 2018, **32**, 2109–2130.
14 D. Y. Yang, T. C. Wang, M. Long and P. Li, *Oxid. Med. Cell. Longevity*, 2020, **2020**, 8825387.
15 R. V. Patel, B. M. Mistry, S. K. Shinde, R. Syed, V. Singh and H. S. Shin, *Eur. J. Med. Chem.*, 2018, **155**, 889–904.
16 R. Z. Tan, C. Wang, C. Deng, X. Zhong, Y. Yan, Y. Luo, H. Y. Lan, T. He and L. Wang, *Phytother. Res.*, 2020, **34**, 139–152.
17 Y. Wang, F. Quan, Q. H. Cao, Y. T. Lin, C. X. Yue, R. Bi, X. M. Cui, H. B. Yang, Y. Yang, L. Birnbaumer, X. J. Li and X. H. Gao, *J. Adv. Res.*, 2021, **28**, 231–243.
18 W. Wu, W. Wang, L. Liang, J. Chen, B. Wei, X. R. Huang, X. Wang, X. Yu and H. Y. Lan, *Mol. Ther.*, 2023, **31**, 344–361.
19 Y. J. Moon, L. Wang, R. DiCenzo and M. E. Morris, *Biopharm. Drug Dispos.*, 2008, **29**, 205–217.
20 X. Wang, X. Zhong, J. Li, Z. Liu and L. Cheng, *Chem. Soc. Rev.*, 2021, **50**, 8669–8742.
21 D. W. Jiang, Z. T. Rosenkrans, D. L. Ni, J. Lin, P. Huang and W. B. Cai, *Acc. Chem. Res.*, 2020, **53**, 1869–1880.
22 Q. Chen, Y. Nan, Y. Yang, Z. Xiao, M. Liu, J. Huang, Y. Xiang, X. Long, T. Zhao, X. Wang, Q. Huang and K. Ai, *Bioact. Mater.*, 2023, **22**, 141–167.
23 H. N. Geo, D. D. Murugan, Z. Chik, A. Norazit, Y. Y. Foo, B. F. Leo, Y. Y. Teo, S. Kadir, Y. Chan, H. J. Chai, M. Medel, N. A. Abdullah, E. J. Johns, M. J. Vicent, L. Y. Chung and L. V. Kiew, *J. Controlled Release*, 2022, **343**, 237–254.
24 D. Y. Zhang, H. Liu, K. S. Zhu, T. He, M. R. Younis, C. Yang, S. Lei, J. Wu, J. Lin, J. Qu and P. Huang, *J. Nanobiotechnol.*, 2021, **19**, 266.
25 Y. Y. Jiang, Z. Y. Ding, M. Gao, C. A. X. Chen, P. J. Ni, C. H. Zhang, B. Wang, G. B. Duan and Y. Z. Lu, *Chin. J. Chem.*, 2021, **39**, 3369–3374.
26 B. Jiang and M. M. Liang, *Chin. J. Chem.*, 2021, **39**, 174–180.
27 T. F. Liu, B. W. Xiao, F. Xiang, J. L. Tan, Z. Chen, X. R. Zhang, C. Z. Wu, Z. W. Mao, G. X. Luo, X. Y. Chen and J. Deng, *Nat. Commun.*, 2020, **11**, 2788.
28 H. Wei, D. W. Jiang, B. Yu, D. L. Ni, M. T. Li, Y. Long, P. A. Ellison, C. M. Siamof, L. Cheng, T. E. Barnhart, H. J. Im, F. Q. Yu, X. L. Lan, X. H. Zhu, Q. J. He and W. B. Cai, *Bioact. Mater.*, 2022, **19**, 282–291.

29 D. Y. Zhang, H. Liu, C. Li, M. R. Younis, S. Lei, C. Yang, J. Lin, Z. Li and P. Huang, *ACS Appl. Mater. Interfaces*, 2020, **12**, 56830–56838.

30 Z. Wang, Y. Zhao, Y. Hou, G. Tang, R. Zhang, Y. Yang, X. Yan and K. Fan, *Adv. Mater.*, 2023, e2210144, DOI: **10.1002/adma.202210144**.

31 X. Wang, T. Wu, Y. Yang, L. Zhou, S. Wang, J. Liu, Y. Zhao, M. Zhang, Y. Zhao, H. Qu, H. Kong and Y. Zhang, *J. Nanobiotechnol.*, 2023, **21**, 63.

32 Z. T. Rosenkrans, T. Sun, D. Jiang, W. Chen, T. E. Barnhart, Z. Zhang, C. A. Ferreira, X. Wang, J. W. Engle, P. Huang and W. Cai, *Adv. Sci.*, 2020, **7**, 2000420.

33 Z. Zhu, X. Liu, P. Li, H. Wang, Y. Zhang, M. Liu and J. Ren, *ACS Appl. Mater. Interfaces*, 2023, **15**, 21854–21865.

34 D. W. Jiang, Z. L. Ge, H. J. Im, C. G. England, D. L. Ni, J. J. Hou, L. H. Zhang, C. J. Kutyreff, Y. J. Yan, Y. Liu, S. Y. Cho, J. W. Engle, J. Y. Shi, P. Huang, C. H. Fan, H. Yan and W. B. Cai, *Nat. Biomed. Eng.*, 2018, **2**, 865–877.

35 Q. Zhang, S. Lin, L. Wang, S. Peng, T. Tian, S. Li, J. Xiao and Y. Lin, *Chem. Eng. J.*, 2021, **413**, 127426.

36 T. Hien Bao Dieu, K.-R. Kim, K. T. Hong, T. Voitsitskyi, J.-S. Lee, C. Mao and D.-R. Ahn, *ACS Cent. Sci.*, 2020, **6**, 2250–2258.

37 Q. Chen, F. Ding, S. Zhang, Q. Li, X. Liu, H. Song, X. Zuo, C. Fan, S. Mou and Z. Ge, *Nano Lett.*, 2021, **21**, 4394–4402.

38 A. Milosevic, D. Hauser, R. Lehner, F. Blank, A. Petri-Fink and B. Rothen-Rutishauser, *Adv. Mater.*, 2018, **30**, e1704307.

39 F. Oroojalian, F. Charbgoo, M. Hashemi, A. Amani, R. Yazdian-Robati, A. Mokhtarzadeh, M. Ramezani and M. R. Hamblin, *J. Controlled Release*, 2020, **321**, 442–462.

40 Y. Zhao, M. Pu, Y. Wang, L. Yu, X. Song and Z. He, *J. Controlled Release*, 2021, **336**, 233–251.

41 M. Ferreira-Silva, C. Faria-Silva, M. C. Carvalheiro, S. Simoes, H. S. Marinho, P. Marcelino, M. C. Campos, J. M. Metselaar, E. Fernandes, P. V. Baptista, A. R. Fernandes and M. L. Corvo, *Pharmaceutics*, 2022, **14**, 104.

42 Y. B. Chen, Y. B. Zhang, Y. L. Wang, P. Kaur, B. G. Yang, Y. Zhu, L. Ye and Y. L. Cui, *J. Nanobiotechnol.*, 2022, **20**, 272.

43 Y. Wang, C. Li, Y. Wan, M. Qi, Q. Chen, Y. Sun, X. Sun, J. Fang, L. Fu, L. Xu, B. Dong and L. Wang, *Small*, 2021, **17**, e2101505.

44 B. Bao, H. Liu, Y. Han, L. Xu, W. Xing and Z. Li, *ACS Appl. Mater. Interfaces*, 2023, **15**, 16460–16470.

45 A. G. Casanova, M. Prieto, C. I. Colino, C. Gutiérrez-Millán, B. Ruszkowska-Ciastek, E. de Paz, Á. Martín, A. I. Morales and F. J. López-Hernández, *Int. J. Mol. Sci.*, 2021, **22**, 729.

46 S. Manohar and N. Leung, *J. Nephrol.*, 2018, **31**, 15–25.